

Phase Stability, Electronic, and Optical Properties in *Pcca*, *R3c*, and *Pm-3m* Phases of BiGaO_3 Perovskite

Lahcene Krache, Mohamed Amine Ghebouli, Brahim Ghebouli, Sultan Alomairy, Mounir Reffas, Messaoud Fatmi,* and Tayeb Chihi

Using generalized gradient approximation (GGA) and local density approximation (LDA), the phase stability, electronic, and optical characteristics of BiGaO_3 in the *Pcca*, *R3c*, and *Pm-3m* phases are examined. The structural phase transition can be caused by the few soft modes between *F* and *Z* points in the *R3c* phase. Because it is coupled to isotropic deformation, the bulk modulus of BiGaO_3 is an indicator of its high hardness. When electrons travel from the top of the valence band (*O-2p*) to the bottom of the conduction band (*Ga-4p* or *Bi-6p*), optical transitions are detected. The pyroxene *Pcca* phase of BiGaO_3 is the most stable, according to GGA–Perdew–Burke–Ernzerhof (PBE) total energy calculations. At 5 GPa, the phase change from the *Pcca* to the *R3c* structure occurs. Because of the smaller reticular lengths and higher Coulomb forces, the elastic constants of BiGaO_3 are quite significant.

1. Introduction

The phase transition mechanism has received considerable attention due to its great technological relevance in steels, ferromagnetic shape memory alloys, and ferroelectric crystals. The phase transitions are due to crystal anisotropy and the relative displacement of atoms in the new phase with respect to that in the parent one. Bismuth gallium oxide is a perovskite, a less hazardous alternative to ferroelectric materials with high ferroelectric polarizations^[1,2] and piezoelectric responses.^[3] At 5 GPa, the phase change from the *Pcca* to the *R3c* structure occurs. Because of the smaller reticular lengths and higher Coulomb forces, the elastic constants of BiGaO_3 are quite significant. BiGaO_3 was studied for a tetragonal structure,^[4] and a ferroelectric polarization of 151.9 C cm^{-2} was discovered. The findings of the experiments show that BiGaO_3 has a pyroxene structure with the space group *Pcca*. Thin single-crystal layers of BiGaO_3 with an orthorhombic structure are created using the sol–gel process.^[5] BiGaO_3 can be adapted to solar systems using ellipsometric measurements of an indirect bandgap.^[5] At 3.2, 6.3, and 9.8 GPa, Yusa et al.^[6] described that BiGaO_3 experiences three pressure-induced phase changes from pyroxene (*Pcca* space group) to perovskite-like monoclinic *Cm*, then to orthorhombic *Cmcm*, and finally to *Pbam* structure. At 3.5, 5.2, and 7.4 GPa, the phase transitions from pyroxene *Pcca* to monoclinic *Cm*, monoclinic *Cm* to rhombohedra *R3c*, and *R3c* to *Pnma* occur.^[4] BiGaO_3 may be produced at high temperatures and pressures.^[7] Hydrostatic pressure, according to Guennou et al., causes the change from the rhombohedra to orthorhombic phase in BiFeO_3 .^[8] The phase stability, the vibrational characteristics, and electronic and optical characteristics of different crystallographic phases of BiGaO_3 under high pressure are described in this article.

2. Calculation Model

The electronic band structure was solved using density functional theory (DFT) within the augmented planewave (APW) approach,^[9] which converges quite quickly as implemented in the CASTEP code.^[10] Brillouin zone integrations were carried out with 660 eV cutoff energy and $8 \times 8 \times 8$ and $6 \times 6 \times 6$ *k*-point grids for cells with 10- (*R3c*) and 20- (*Pcca*) to guarantee that structure


L. Krache
PQSD Laboratory
Department of Physics, Faculty of Science
University Ferhat Abbas of Setif 1
Setif 19000, Algeria

M. A. Ghebouli
Department of Chemistry
Faculty of Technology
University of Mohamed Boudiaf
M'sila 28000, Algeria

M. A. Ghebouli, M. Reffas, M. Fatmi, T. Chihi
Research Unit on Emerging Materials (RUEM)
University Ferhat Abbas of Setif 1
Setif 19000, Algeria
E-mail: m.fatmi@univ-setif.dz

B. Ghebouli
Laboratory of Studies Surfaces and Interfaces of Solids Materials
Department of Physics
Faculty of Science
University Ferhat Abbas of Setif 1
Setif 19000, Algeria

S. Alomairy
Department of Physics
College of Science
Taif University
P.O. Box 11099, Taif 21944, Saudi Arabia

 The ORCID identification number(s) for the author(s) of this article can be found under <https://doi.org/10.1002/pssb.202200042>.

DOI: 10.1002/pssb.202200042

and energies were properly converged. Within generalized gradient approximation (GGA) of the Perdew–Burke–Ernzerhof (GGA–PBE) functional^[11] and local density approximation (LDA),^[12] the cell shape and internal atomic locations were tuned. The structures in question were relaxed by reducing their enthalpy at pressures ranging from 0 to 10 GPa. The utilization of $20 \times 20 \times 20$ uniform k -points is required for the computation of optical characteristics. The Broyden–Fletcher–Goldfarb–Shanno (BFGS) minimization technique was used to determine the structural parameters.^[13–16] Total energy 5×10^6 eV atom⁻¹, maximum ionic Hellmann–Feynman force 10^{-2} eV Å⁻¹, and maximum stress 2×10^{-2} eV Å⁻³ were the tolerances for geometry optimization.

3. Results and Discussions

3.1. Phase Stability

Using GGA and LDA approximations, we investigated the structural behavior of BiGaO₃ in pyroxene *Pcca*, rhombohedra *R3c*, and *Pm-3m* phases. Table 1 shows the atomic locations of their

Table 1. The atomic positions of Bi, Ga, and O atoms in *R3c*, *Pcca*, and *Pm-3m* phases of BiGaO₃.

	Atom	Atomic positions		
<i>R3c</i> phase	Bi	0.213	0.213	0.213
	Ga	0.489	0.489	0.489
	O	0.178	0.317	0.773
<i>Pcca</i> phase	Bi	0	0.25	0.890
	Ga	0.50	0.75	0.356
	O	0.232	0.904	0.946
<i>Pm-3m</i> phase	Bi	0	0	0
	Ga	0.50	0.50	0.50
	O	0	0.50	0.50

Table 2. The lattice parameters, bulk modulus, and its pressure derivative (calculated from Birch–Murnaghan) for BiGaO₃ perovskite.

	References	a [Å]	b [Å]	c [Å]	B_0 [GPa]	B'
<i>Pm-3m</i>	GGA This work	3.8988 ^{a)}	–	–	172.74 ^{a)}	4.40 ^{a)}
	LDA	3.8147 ^{a)}			215.21 ^{a)}	4.38 ^{a)}
	Other	3.899 ^[17]			206.87 ^[17]	
<i>Pcca</i>	GGA This work	5.508	5.177	10.198	76.16	4.52
	LDA	5.353	5.095	9.793	78.06	4.32
	Exp	5.626 ^[5]	5.224 ^[5]	10.339 ^[5]		
	Other	5.503 ^[4]	5.195 ^[4]	10.112 ^[4]		
<i>R3c</i>	GGA This work	5.671	5.671	5.671		
	LDA	5.492	5.492	5.492	93.74	4.02
	Other	5.557 ^[4]	5.557 ^[4]	5.557 ^[4]	95.67	4.25

^{a)}From Birch–Murnaghan.

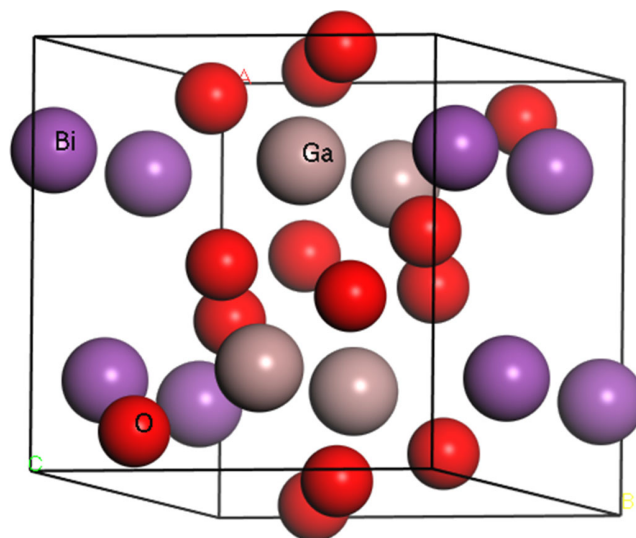


Figure 1. The *Pcca* structure of BiGaO₃ phase.

various constituents (Bi, Ga, and O). Table 2 shows the lattice constants, bulk modulus, and pressure derivative for the *Pcca*, *R3c*, and *Pm-3m* phases. For the *Pm-3m* phase, the lattice constant is closer to the theoretical value.^[17] The crystal structure of the more stable phase pyroxene *Pcca* of BiGaO₃ compound is shown in Figure 1. Within the generalized gradient approximation, we show the total energies of fully optimized aforementioned phases of BiGaO₃ at ambient pressure in Figure 2. According to GGA-total PBE's energy estimates, the pyroxene *Pcca* phase is more stable than *R3c* and *Pm-3m*. The plots of normalized volume on pressure for the *R3c*, *Pcca*, and *Pm-3m* phases of BiGaO₃ are shown in Figure 3, with the *Pcca* phase showing the most stability. As the crystallographic ground state of BiGaO₃, the GGA–PBE appropriately predicts the pyroxene phase. Figure 4 shows the effect of pressure on the formation

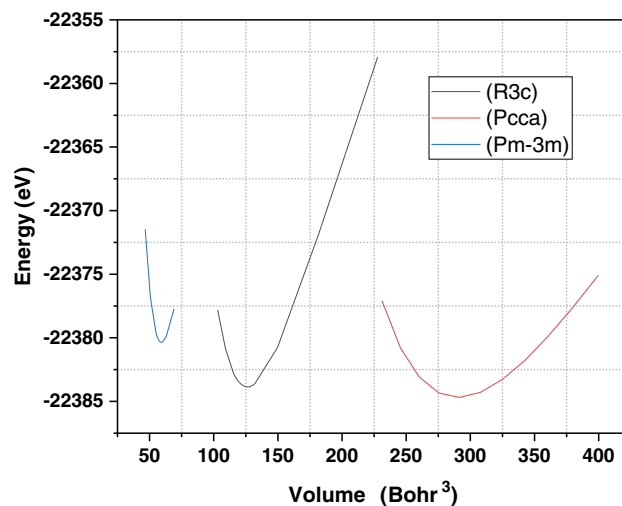


Figure 2. The impact of volume on total energy for *R3c*, *Pcca*, and *Pm-3m* phases of BiGaO₃.

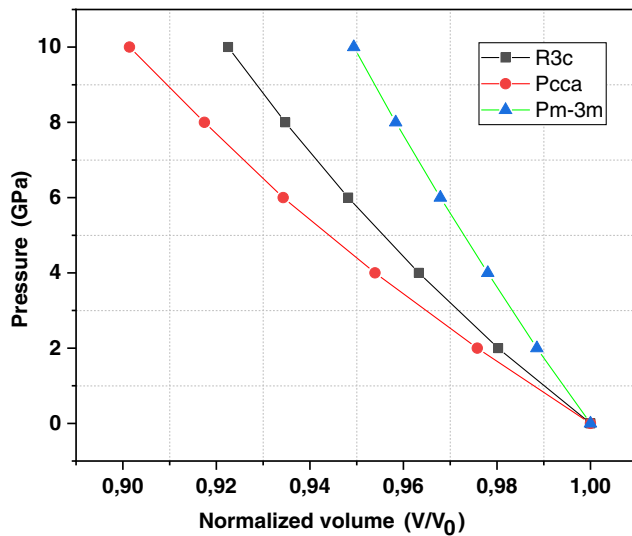


Figure 3. The impact of normalized volume on pressure for *R3c*, *Pcca*, and *Pm-3m* phases of BiGaO_3 .

enthalpy of the *R3c* and *Pcca* phases of BiGaO_3 . At 5 GPa, the phase change from the *Pcca* to the *R3c* structure occurs. In contrast to our findings, the minimal enthalpy route of the investigated phases is $Pcca \rightarrow Cm \rightarrow R3c \rightarrow Pnma$, with phase transitions occurring at 3.5, 5.2, and 7.4 GPa.^[4] **Table 3** shows the elastic moduli for the BiGaO_3 phases *Pcca*, *Pm-3m*, and *R3c*. The LDA elastic constants match theoretical values stated in the literature^[17] fairly well. For the first time, the elastic constants of the BiGaO_3 compound in the *Pcca* and *R3c* phases have been computed. When compared with the GGA approximation, the LDA approximation yields greater elastic constants. The bulk modulus computed using the Birch Murnaghan fit is said to be identical to that derived using elastic constants. The vibrational characteristics were obtained using the direct technique. **Figure 5** depicts the phonon band structure for *Pcca*, *R3c*, and *Pm-3m* phases. For *R3c* phase, it indicates a soft mode between *F* and *Z* direction. The structural phase change could be caused by this soft mode. The *Pcca* phase is dynamically stable, but the *Pm-3m* phase is unstable, according to the vibrational perspective

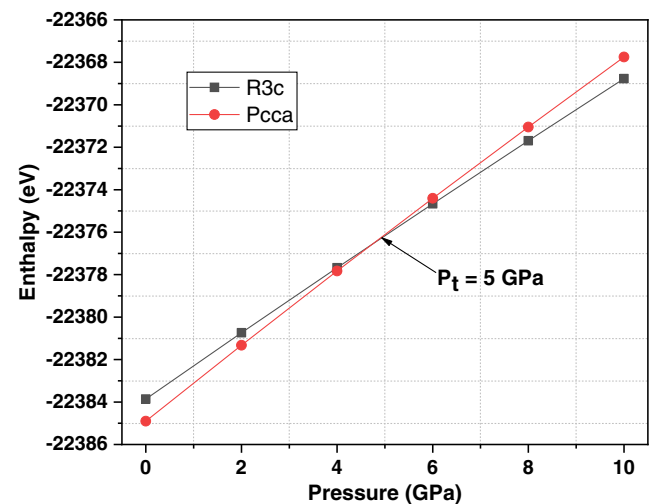


Figure 4. The impact of pressure on formation enthalpy for *R3c* and *Pcca* phases of BiGaO_3 .

of phonons. BiGaO_3 has significant elastic constants due to its short reticular distances and higher Coulomb forces, which explain its hardness.

3.2. Density of States and Band Structure

The results of the electronic band structure simulations for BiGaO_3 in the pyroxene *Pcca*, rhombohedra *R3c*, and cubic *Pm-3m* phases are shown in **Figure 6**. The bands in the first two phases of the band structure have a similar form. The band gap for GGA (LDA) is direct $X \rightarrow X$: 1.953 eV (1.960 eV) in the *Pcca* phase, direct $\Gamma \rightarrow \Gamma$: 2.958 eV (2.918 eV) in the *R3c* phase, and indirect $M \rightarrow X$: 1.015 eV (1.155 eV) in the *Pm-3m* phase. The theoretical bandgap in the *R3c* phase, calculated using the extended gradient approximation,^[18] is 1.88 eV. **Figure 7** shows the total and partial density of states for the *Pcca*, *R3c*, and *Pm-3m* phases with energies ranging from -10 to $+10$ eV. The valence band is divided into two sections. The *O-2p* states dominate the upper valence band below the

Table 3. The computed elastic moduli (GPa) for *Pcca*, *Pm-3m*, and *R3c* BiGaO_3 phases.

		C_{11}	C_{12}	C_{44}	C_{22}	C_{33}	C_{55}	C_{66}	C_{23}	C_{13}	C_{14}
<i>PCCA</i> ^{a)}	GGA	164.1	68.3	61.40	163.7	94.48	39.98	53.83	70.32	42.42	–
	LDA	184.6	83.4	71.1	197.2	111.9	31.1	58.8	91	57.7	–
<i>Pm-3m</i>	GGA	279.5	115.8	92.3	–	–	–	–	–	–	–
	LDA	355.0	145.3	105.5	–	–	–	–	–	–	–
	Other ^[17]	292.2	115.1	96.7	–	–	–	–	–	–	–
<i>R3c</i>	GGA	212.1	108.5	31.8	–	150.8	–	–	–	36	26.4
	LDA	261.8	144.5	49.5	–	–	–	–	–	63.7	27

^{a)}From elastic constants

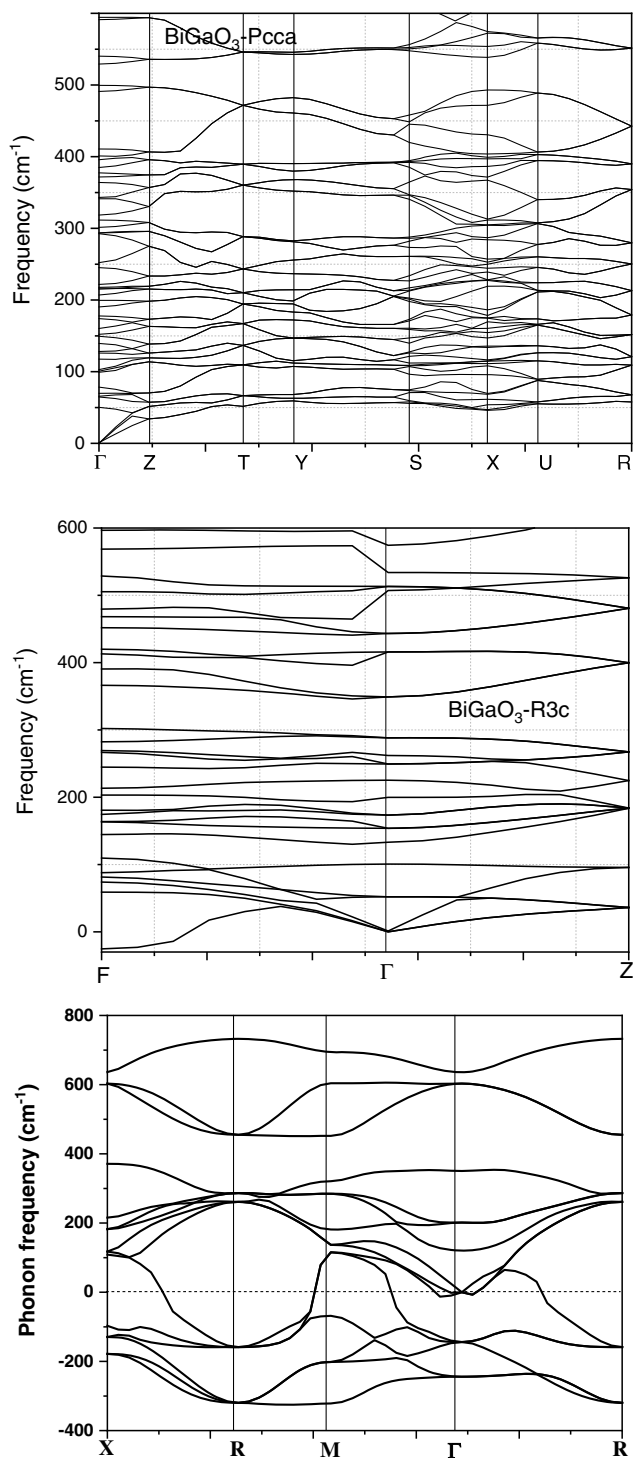


Figure 5. The phonon band structure of BiGaO_3 in the *Pcca*, *R3c*, and *Pm-3m* phases.

Fermi level, with modest contributions from the Ga-3*p* and Bi-6*p* levels. Bi-6*s* states appear below these bands, with tiny contributions from O-2*p* states and Ga-*s*. Between Fermi's level and 3.5 eV, the first conduction band is vacant. Near the Fermi level, the occupied Bi-6*s* and O-2*p* states form antibonding

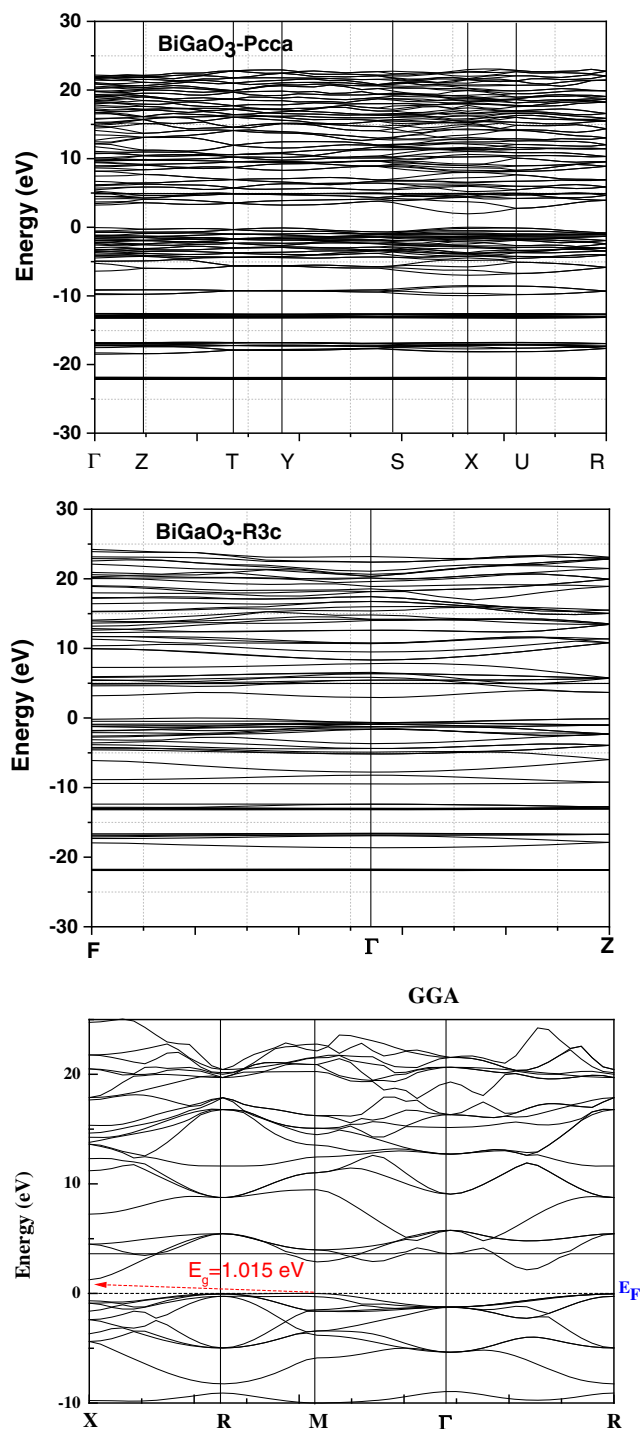


Figure 6. The electronic band structure for BiGaO_3 in the *Pcca*, *R3c*, and *Pm-3m* phases.

states. Noncentrosymmetric *R3c* perovskite antibonding states hybridize with Bi-6*p* states in centrosymmetric *Pcca* pyroxene, resulting in an asymmetric electron distribution around the Bi atoms. In the generation of lone pairs, the scenario for *Pcca* and *R3c* is typical.^[19] Due to the centrosymmetric structure of *Pcca*

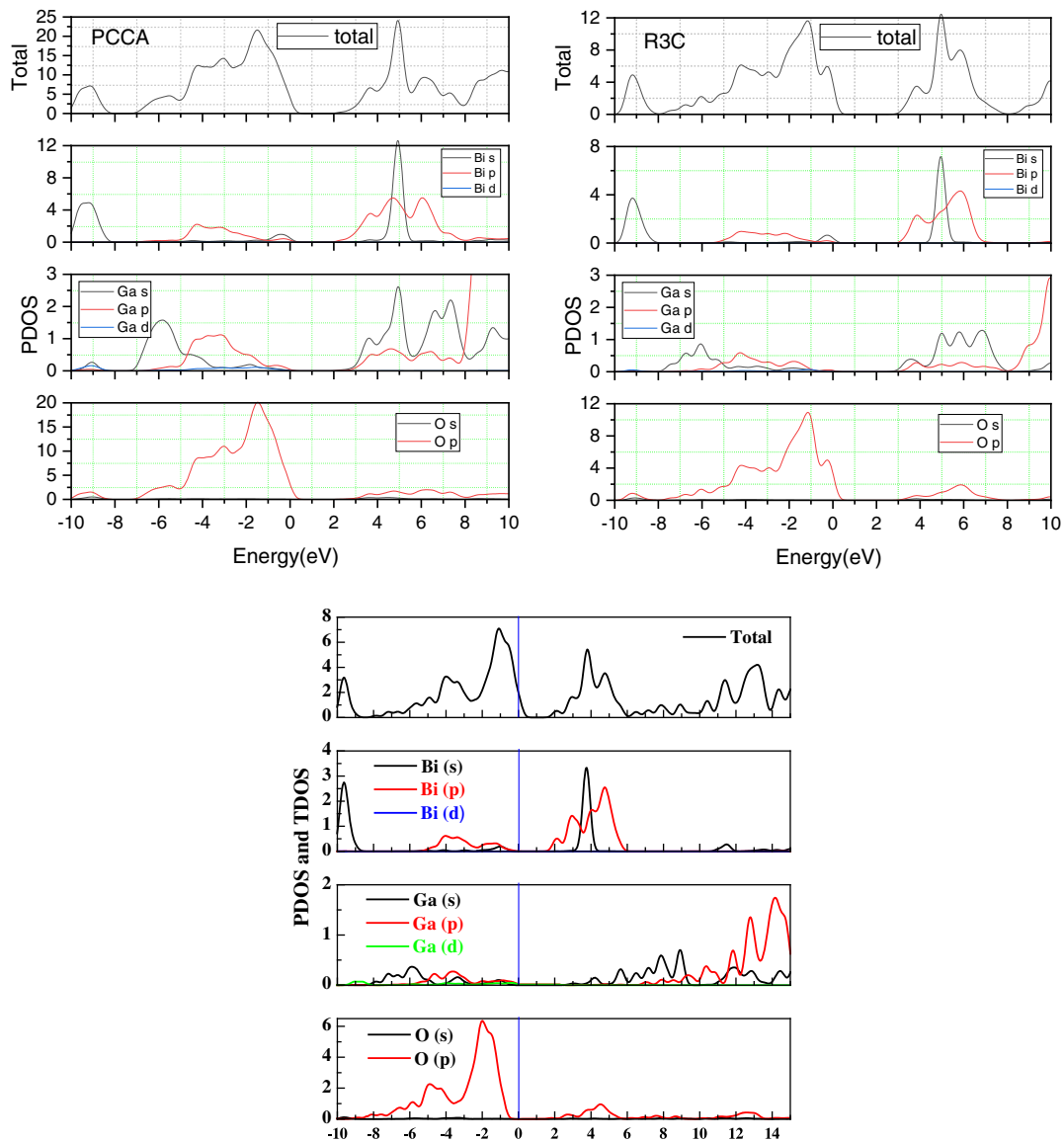


Figure 7. The density of states for BiGaO_3 in the *Pcca*, *R3c*, and *Pm-3m* phases.

pyroxene, the lone pairs are organized in the opposite direction. The lone pairs in rhombohedra *R3c* promote structural distortion, making this phase ferroelectric.

3.3. Optical Properties

The study of transitions from six upper valence bands to seven lower conduction bands necessitates knowledge of the imaginary part of the dielectric function, which we show in **Figure 8** (right panel) as a function of photon energy. The dielectric function, $\epsilon(\omega) = \epsilon_1(\omega) + \epsilon_2(\omega)$, is a fundamental optical parameter that describes the material's polarization and absorption, where $\epsilon_1(\omega)$ and $\epsilon_2(\omega)$ are the real and imaginary parts of the dielectric function, respectively. The momentum matrix between the occupied and unoccupied electronic states

can be used to calculate the imaginary portion $\epsilon_2(\omega)$. In **Figure 8** (left panel), the transition energy is displayed, where i and j are the valence and conduction band levels. The imaginary part threshold energy is 2.85 and 1.85 eV, respectively, which are the fundamental direct bandgaps of BiGaO_3 in the *Pcca* and *R3c* phases. Transitions from an occupied O-2p orbital to an unoccupied Bi-6p or Ga-4p orbital are investigated. For the *Pcca* and *R3c* phases, all peaks in the imaginary part correspond to potential transitions given in **Table 4** and **5**. The reflectivity, absorption, and loss function for BiGaO_3 in the *Pcca* and *R3c* phases are plotted in **Figure 9**. BiGaO_3 has a reflectance of 0.025%, which corresponds to a wavelength of 25 nm. It reaches a maximum value of 0.35% and 0.32% at 75 and 250 nm for *R3c* and *Pcca* phases, respectively, after repeated organization. Under UV light irradiation, the phototransition energies from

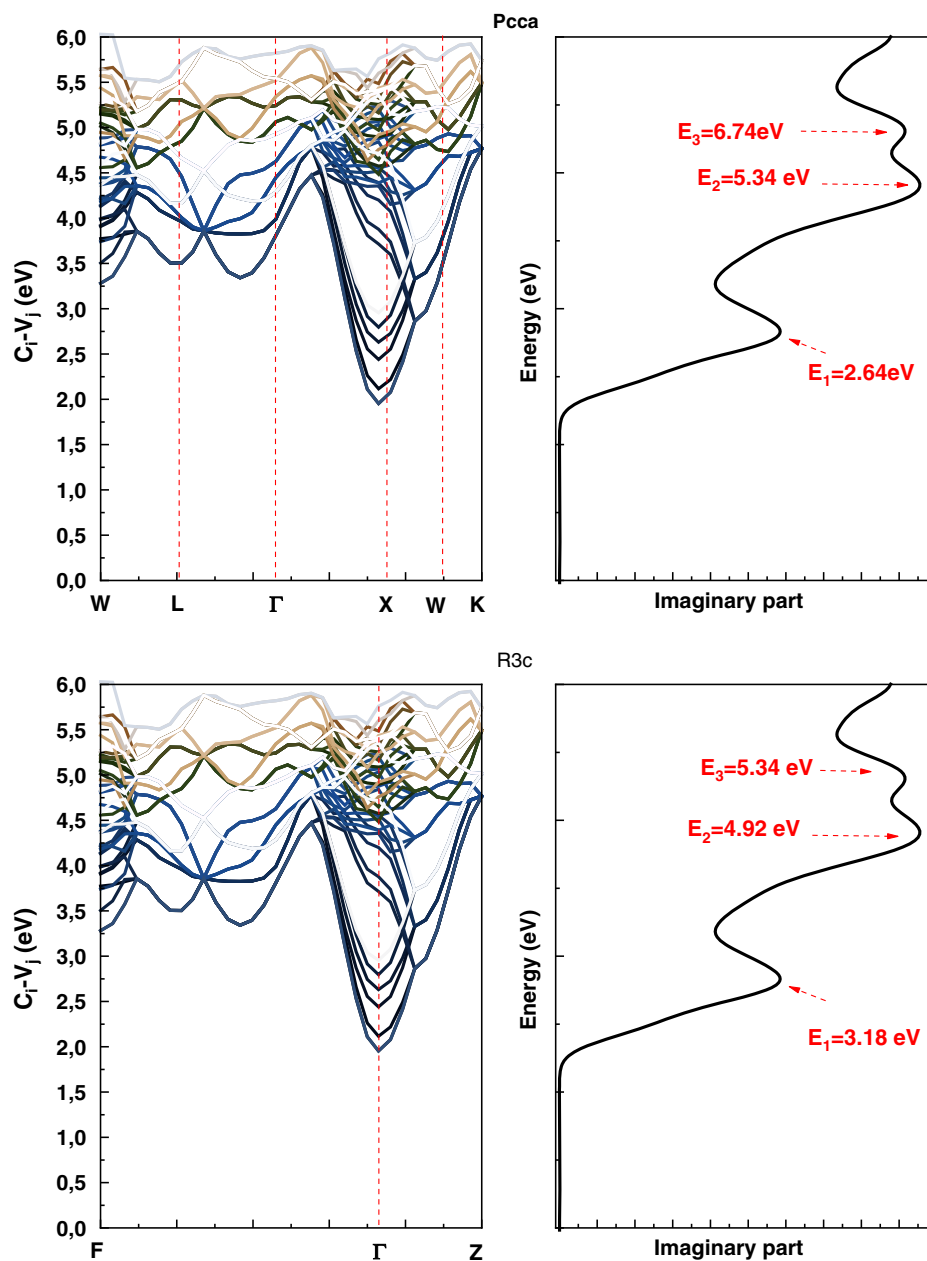


Figure 8. The transition energy $E(k) = E_{c_j}(k) - E_{v_i}(k)$ (left panel) and imaginary part of dielectric function (right panel) for BiGaO_3 in the $Pcca$ and $R3c$ phases.

Table 4. The possible transitions that correspond to the peaks of the imaginary dielectric constant for the $Pcca$ phase.

BiGaO_3	$E = 2.64 \text{ eV}$	$E = 5.34 \text{ eV}$	$E = 6.74 \text{ eV}$
$Pcca$	$V_4 \rightarrow C_2; V_3 \rightarrow C_7$ at X point	$V_4 \rightarrow C_5; V_2 \rightarrow C_5$ $V_3 \rightarrow C_6; V_1 \rightarrow C_4$ at Γ point	$V_6 \rightarrow C_3; V_4 \rightarrow C_7$ $V_2 \rightarrow C_7; V_6 \rightarrow C_4$ at U point

Table 5. The possible transitions that correspond to the peaks of the imaginary dielectric constant for the $R3c$ phase.

BiGaO_3	$E = 3.18 \text{ eV}$	$E = 4.92 \text{ eV}$	$E = 5.34 \text{ eV}$
$R3c$	$V_5 \rightarrow C_1; V_4 \rightarrow C_1$ at Γ point	$V_2 \rightarrow C_7; V_3 \rightarrow C_6$ $V_1 \rightarrow C_7; V_1 \rightarrow C_5$ at Γ point	$V_6 \rightarrow C_3; V_4 \rightarrow C_7$ at Γ point $V_2 \rightarrow C_7; V_6 \rightarrow C_4$ at F point

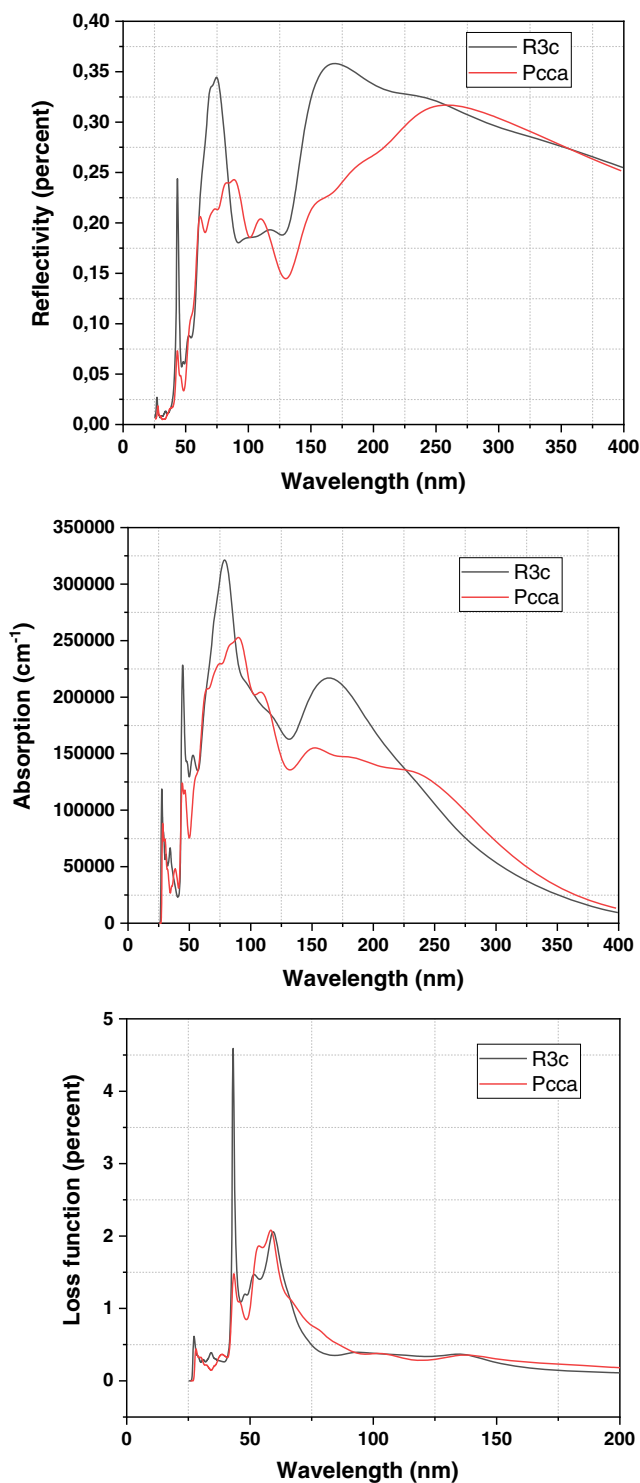


Figure 9. The reflectivity, absorption, and loss function for BiGaO₃ in the *Pcca* and *R3c* phases.

maximum valence band to minimum conduction band are assigned to the absorption peaks. At wavelengths of 75 and 100 nm, the high value of absorption for *R3c* and *Pcca* phases is 325 000 and 250 000 cm⁻¹, respectively. BiGaO₃ has a high absorption value, indicating that it could be used as a

photocatalyst. Between 4.5% and 2% is the high loss function. The reduced loss energy corresponds to wavelengths between 45 and 60 nm and can reveal information about the composition and electronic structure.

4. Conclusion

The first-principles method was used to investigate the ground-state characteristics as well as the high-pressure behavior of BiGaO₃. The development of the lone pair in the region of the bismuth atoms and, as a result, ferroelectric characteristics is due to the mixing of Bi-*s*, Bi-*p*, and O-*p* states near the top of the valence band. BiGaO₃ is a semiconductor, according to the GGA direct-bandgap X → X (1.953 eV) in *Pcca* phase, direct-bandgap $\Gamma \rightarrow \Gamma$ (2.958 eV) in *R3c* phase, and indirect-bandgap M → X (1.015 eV) in *Pm-3m* phase. Near the Fermi level, the occupied Bi-6s and O-2p states form antibonding states. For the first time, the elastic constants of the BiGaO₃ compound in *Pcca* and *R3c* have been computed. BiGaO₃ is a possibility for photocatalyst material due to its high absorption value.

Acknowledgements

The authors would like to thank Taif University Research Supporting project number (TURSP-2020/63), Taif University, Taif, Saudi Arabia.

Conflict of Interest

The authors declare no conflict of interest.

Data Availability Statement

Research data are not shared.

Keywords

band structures, BiGaO₃ perovskites, optical absorption, *Pcca* phases, *R3c* phases

Received: January 29, 2022

Revised: April 28, 2022

Published online: May 26, 2022

- [1] N. A. Hill, K. M. Rabe, *Phys. Rev. B* **1999**, *59*, 8759.
- [2] R. Seshadri, N. A. Hill, *Chem. Mater.* **2001**, *13*, 2892.
- [3] F. Akram, R. A. Malik, S. A. Khan, A. Hussain, S. Lee, M. H. Lee, C. H. In, T. K. Song, W. J. Kim, Y. S. Sung, M. H. Kim, *J. Electroceram.* **2018**, *41*, 93.
- [4] J. Kaczowski, *J. Mater. Sci.* **2016**, *51*, 9761.
- [5] J. Z. Zhang, H. C. Ding, J. J. Zhu, Y. W. Li, Z. G. Hu, C. G. Duan, X. J. Meng, J. H. Chu, *J. Appl. Phys.* **2014**, *115*, 0831110.
- [6] H. Yusa, A. A. Belik, E. Takayama-Muromachi, N. Hirao, Y. Ohishi, *Phys. Rev. B* **2009**, *80*, 214103.
- [7] A. A. Bellik, T. Wuemisch, K. Mori, M. Maic, T. Nagai, Y. Matsui, E. Takayama-Muromachi, *Chem. Mater.* **2006**, *18*, 133.
- [8] M. Guennou, P. Bouvier, G. S. Chen, B. Dkhil, R. Haumont, G. Garbarino, J. Kreisel, *Phys. Rev. B* **2011**, *84*, 174107.

- [9] K. M. Leung, Y. F. Liu, *Phys. Rev. B* **1990**, *41*, 10188.
[10] M. D. Segall, P. J. D. Lindan, M. J. Probert, C. J. Pickard, P. J. Hasnip, S. J. Clark, M. C. Payne, *J. Phys.: Condens. Matter* **2002**, *14*, 2717.
[11] J. P. Perdew, K. Burke, M. Ernzerhof, *Phys. Rev. Lett.* **1986**, *77*, 3865.
[12] J. P. Perdew, A. Zunger, *Phys. Rev. B* **1981**, *23*, 5048.
[13] C. G. Broyden, *J. Inst. Math. Appl.* **1970**, *13*, 76.
[14] R. Fletcher, *Comput. J.* **1970**, *13*, 317.
[15] D. Goldfarb, *Math. Comput.* **1970**, *24*, 23.
[16] D. F. Shanno, *Math. Comput.* **1970**, *24*, 647.
[17] R. B. Behram, M. A. Iqbal, S. M. Alay-e-Abbas, M. Sajjad, M. Yaseen, M. I. Arshad, G. Murtaza, *Mater. Sci. Semicond. Process.* **2016**, *41*, 297.
[18] J. Kaczkowski, *J. Alloys Compd.* **2014**, *613*, 175.
[19] A. Walsh, D. J. Payne, R. G. Egdell, G. W. Watson, *Chem. Soc. Rev.* **2011**, *40*, 4455.